A MOLECULAR DYNAMICS STUDY OF STRUCTURAL AND DYNAMIC PROPERTIES OF GOLD NANOPARTICLES WITH PALLADIUM COATING

Unal Domekeli[1], Sedat Sengul[1], Murat Celtek[2]

[1]*Dept. of Physics, Trakya University, 22030, Edirne – TURKEY*
[2]*Faculty of Education, Trakya University, 22030, Edirne – TURKEY*

Abstract

In this work, we presented an investigation on the melting process of gold (Au) nanoparticles with palladium (Pd)-coating by using molecular dynamics (MD) simulations at the nanoscale. Interatomic interactions in MD simulations were described using the embedded atom method (EAM)-based Sutton - Chen (SC) potentials. In order to monitor the melting process of nanoparticles, we examined the temperature-dependent changes of physical properties such as potential energy, pair distribution functions and diffusion coefficients. In addition, the dynamics in the structure of the nanoparticle was investigated by visualizing the atomic configurations obtained from the MD simulations. The results show that the melting point of Au nanoparticle with Pd-coating is smaller than that of bulk Au but higher than that of uncoated Au nanoparticle. The reason why the Au nanoparticle with Pd-coating has a higher melting point than the uncoated Au particle is that the epitaxial Au/Pd interface causes overheating of the nanoparticle by suppressing the melt nucleation and growth.

Keywords: Molecular dynamics simulations, core/shell metallic nanoparticle, melting temperature.

INTRODUCTION

Bi-metallic nanoparticles are nano-materials with a core/shell structure consisting of different types of atoms. These nano-materials have been the focus of many researchers due to their unique physical and chemical properties that are not observed in mono-metallic and bulk materials [1-3]. This new material family is needed in the micro-electronics industry due to the increasing use of low-size materials and the thermal stability of bi-metallic nanoparticles against melting. In particular, these materials are used in many application areas of nanotechnology such as sensors, semiconductors, bio-markers, nano-catalysis and optoelectronics [4-9]. Therefore, understanding the thermal stability, melting mechanism and structural properties of bi-metallic materials plays an important role in miniaturization of these materials.

Real-time observation and analysis of the physical mechanisms underlying many special characteristics of the dynamic, structural and thermodynamic properties of bi-metallic nanoparticles (NP) are not readily available experimentally. Due to the rapid development of computational algorithms and available computational resources for small-sized nanocrystals, MD simulations, along with other computational methods, occupies an increasingly important place in this rapidly developing and expanding field [10]. Therefore, MD simulations are a suitable tool for investigating the structural evolution of metallic nanocrystals under the influence of temperature at the atomic scale [11]. Recently, many researchers have reported studies on the melting mechanism of bi-metallic nano-materials using MD simulations [11-17]. For example, Zhang et al. [14] reported superheating of lead nanofilm (NF) in an aluminum matrix using MD simulation. Shvets et al. [16] studied the thermal stability of metallic NPs with a core-shell structure. Shi et al. [17] investigated the melting process of silver nanowire (NW) with nickel coating by using MD simulation. They reported that silver NWs with nickel coating overheats like NPs

and NFs. In this study, we present a MD simulation study on the thermal, structural and dynamic properties of Au NPs with Pd-coating.

EXPOSITION

In this study, all MD simulations for Au NPs with Pd-coating were performed using the parallel code of DL_POLY 2.0 [18] MD simulation package. The success of classical MD simulations depends to a large extent on the pair potential that define the interaction between atoms in the system. SC potential was used to describe interactions between atoms in MD simulations. Based on the SC potential, the total potential energy of a finite system with N atoms is written as [19]

$$U_{tot} = \sum_i U_i , \tag{1}$$

$$U_i = \sum_i \varepsilon \left[\sum_{j \neq i} \frac{1}{2} V(r_{ij}) - c \, \rho_i^{1/2} \right] , \tag{2}$$

$$V(r_{ij}) = \left(\frac{a}{r_{ij}} \right)^n , \tag{3}$$

$$\rho_i = \sum_{j \neq i} \varphi(r_{ij}) = \sum_{j \neq i} \left(\frac{a}{r_{ij}} \right)^m \tag{4}$$

where r_{ij} is the distance between the atoms i and j, and $V(r_{ij})$ is the pair potential between the atoms representing repulsive interactions in total energy. ρ_i is the energy density function of the atom i, representing the attractive term in total energy. To construct the potential for the binary alloy state, Au-Pd from the corresponding SC potentials for the elemental state, we used the following combination rule [20,21].

$$a_{ij} = \frac{a_i + a_j}{2} , \tag{5}$$

$$\varepsilon_{ij} = \sqrt{\varepsilon_i \varepsilon_j} , \tag{6}$$

$$n_{ij} = \frac{n_i + n_j}{2} , \tag{7}$$

$$m_{ij} = \frac{m_i + m_j}{2} . \tag{8}$$

In this study, the parameters of the quantum SC (QSC) potential, which were the re-

parameterized form of SC potential by Cagin et al. [20], were used. The QSC potential parameters ε, c, a, n and m for Au and Pd are listed in Table 1 [20].

Table 1. *The QSC potential parameters for Pd and Au [20].*

Metal	n	m	ε (eV)	c	a (Å)
Pd	12	6	3.2864×10^{-3}	148.205	3.8813
Au	11	8	7.8052×10^{-3}	53.581	4.0651

A model NP with core (Au)/shell (Pd) structure used in MD simulations were obtained by cutting from a large face-centered cubic (fcc) structure. The Au NPs was coated by Pd in a "cube on cube" orientation, that is Au[100]//Pd[100], Au[110]//Pd[110], and so on. In this study, two different configurations of NPs with core/shell structure were used to investigate the shell effect. A sample of the initial atomic configuration of Au NP with Pd-coating is displayed in Figure 1. We also simulated Au NP without coating to perform a comparison. The numbers of atom of the NPs used in the simulations are listed in Table 2. In addition, simulations of the bulk system were performed with 5324 Au atoms.

Table 2. *The number of atoms of NPs used in MD simulations.*

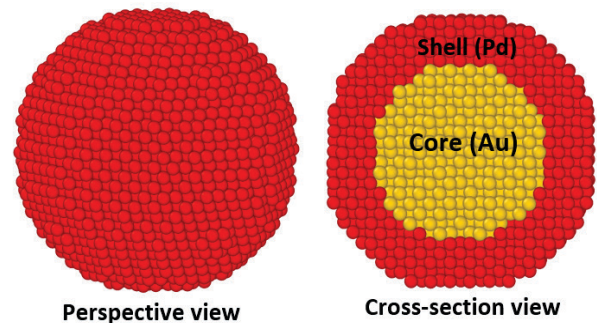| Number of atoms	Coated NP-1	Coated NP-2	Uncoated NP
Total	5769	5769	5769
Core (Au)	3511	1433	
Shell (Pd)	2258	4336	

Fig. 1. *Perspective and cross-sectional image representation of the atomic configuration of the model Au NP with Pd-coating.*

To account for the surface effects of the NPs, the periodic boundary conditions in the MD

simulations were not applied in any direction. The samples with atoms in ideal fcc positions were relaxed with the following annealing period: first, the system was heated to 300 K with a heating rate of 0.05 K/ps, and then cooled to 0 K using the same rate. NPs were simulated under the constant volume and constant temperature (NVT) canonical ensemble. For the bulk system, MD simulations were performed under isothermal-isobaric (NPT) ensemble with periodic boundary conditions. From 100 to 1800 K for NPs and bulk, each system was subjected to a heating treatment consisting of a series of MD simulations with a temperature increase of ΔT = 100 K. Around the melting point, the temperature increment was reduced to ΔT =10 K, taking into account large temperature fluctuations. For each simulation, 50 ps was employed for equilibration followed by 50 ps production time to produce time-based properties at each temperature. The classical equations of motion were integrated using the Leapfrog Verlet method with a time step of 1 fs. The desired temperature and ambient pressure were controlled by the Nose-Hoover thermostat and Berendsen [22,23] approach, respectively.

The phase of the system can be determined by examining the characteristic behavior of the pair distribution function (PDF). The expression of the PDF, $g(r)$, is as follows [21]:

$$g(r) = \frac{\Omega}{N^2} \left\langle \sum_i^N \sum_{i \neq j}^N \delta(r - r_{ij}) \right\rangle \qquad (9)$$

where N and Ω represent the number of atoms, and volume of the simulations cell, respectively. In order to test the accuracy of the potential functions used to describe the interactions between atoms in MD simulations, the PDF obtained from the MD for bulk Au in Figure 2 was compared with the experimental data [24]. As can be seen from Figure 2, the MD result is in very good agreement with the experimental one. This result shows that the QSC potential accurately describes Au-Au interactions in MD simulations. Also, both MD and experimental PDFs show the characteristic behavior of liquid phase. The best-known way for observing the first-order phase transition during the heating process in NPs and the bulk system is to monitor the variation of the energetic curve with temperature.
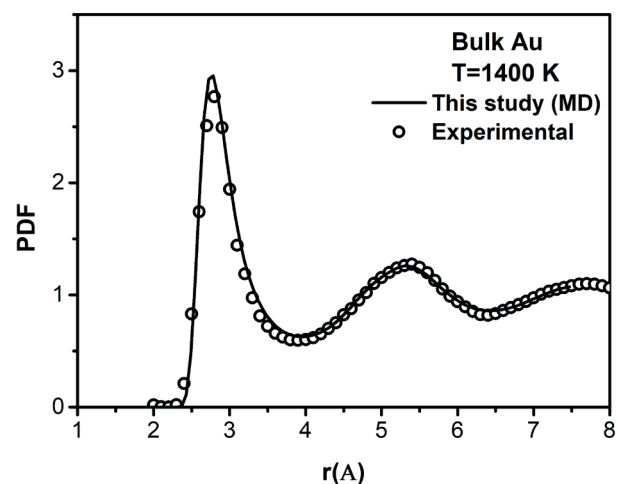

Fig. 2. *The PDFs of liquid bulk Au simulated under 0 GPa pressure at 1400 K (experimental data under 0 GPa pressure at 1423 K[24]).*

Generally, the temperature at which the sudden change in this curve occurs is defined as the melting point of the system. In this study, the melting temperature of the NPs and the bulk system was determined following this method. In this context, the temperature-dependent changes of the potential energies of the uncoated NP, coated NP-1 and NP-2, and the bulk system are shown in Figure 3.
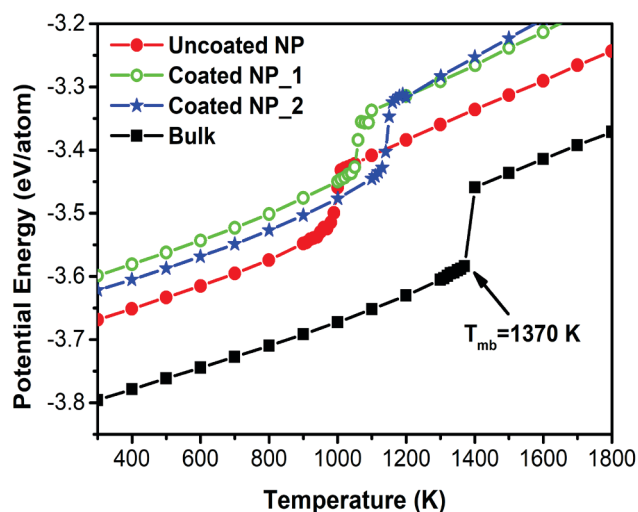

Fig. 3. *Temperature-dependence of the potential energy for Au NPs and bulk system.*

The potential energy curve for each system changes almost linearly with temperature up to their melting point. A sudden increase around melting point is observed in all curves. After the melting point, the potential energy increases linearly with temperature for all systems. For uncoated NP, coated NP-1 and NP-2, and the bulk system, the melting temperatures

546

predicted from the sudden change in potential energy are 990 K, 1050 K, 1140 K, and 1370 K (experimental melting point, $T_{expt.}$=1330 K for bulk Au [25]), respectively. The melting temperature obtained from the MD simulations is in good agreement with the experimental value. This demonstrates the accuracy of the MD results. All NPs have lower melting temperatures than that of bulk. Uncoated NP has the lowest melting temperature while coated NP-2 has the highest one. Also, the potential energy of the bulk is lower than that of NPs at all temperatures. The potential energies of uncoated NP, coated NP-1 and NP-2 at 300 K are -3.66 eV, -3.59 eV and -3.62 eV, respectively. Uncoated NP has the lowest potential energy, while uncoated NP-1 has the largest.

To observe the structural changes of NPs during the melting process, PDFs of uncoated NP, coated NP-1 and NP-2 are given in Figure 4 (a-c), respectively. At 300 K and 900 K, all nanoparticles exhibit narrow and sharp peaks, which are the characteristic behavior of the crystalline phase. With the increase in temperature, the peak heights of the PDFs decrease, while the widths of the peaks increase. As can be seen from Figure 4, the characteristic behavior of PDFs at the melting point of each NPs reflects neither crystalline nor liquid phase. This can be explained by the knowledge that a system has two phases together at its melting point. After the melting point, the PDFs for uncoated NP, coated NP-1 and NP-2 show the characteristic behavior of the liquid phase at 1000 K, 1060 K and 1150 K, respectively.

Diffusion coefficient (D), a measure of atomic mobility, can be obtained from positions and velocities containing atomic trace information in MD simulations. The D is expected to be related to the path taken by the particle over time t. This suggests that the square displacement for large t values is linearly linked. The D can be calculated from the Einstein correlation given as:
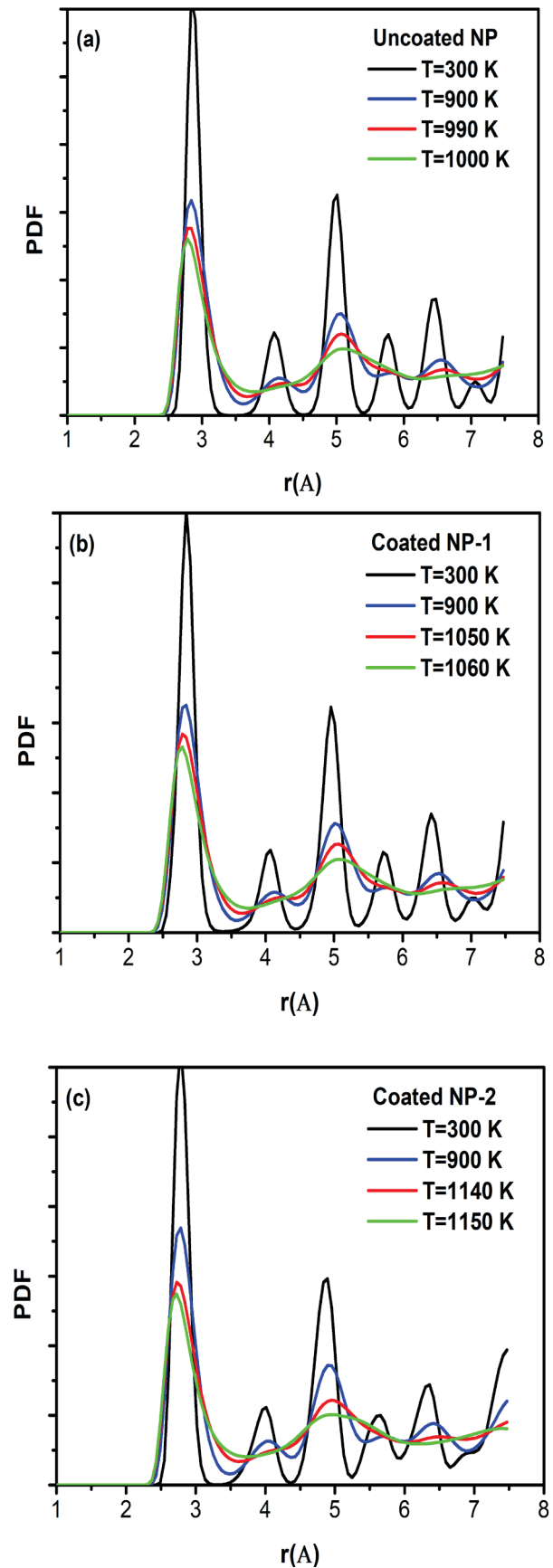
$$D = \frac{1}{6t} lim\langle r^2(t)\rangle .\qquad(10)$$

Fig. 4. *PDFs of (a) uncoated NP, (b) coated NP-1 and (c) NP-2 at different temperatures.*
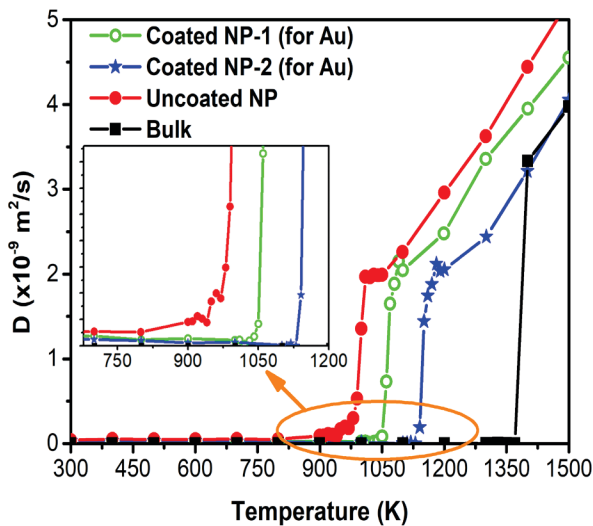
Fig. 5. *Diffusion coefficients of uncoated NP, coated NP-1 and NP-2 as a function of temperature.*

Figure 5 shows the temperature dependent variation of the diffusion coefficients of Au atoms for uncoated NP, coated NP-1 and NP-2. While the Ds of Au atoms are approximately zero at low temperatures for all NPs, a sudden increase in their values is observed at melting points. This increase indicates that the metallic bonds of the Au atoms that make up the NP are broken and they get rid of their lattice and gain mobility. For uncoated NP, Au atoms diffuse at lower temperature, while coated NPs diffuse at higher temperature. As can be seen from the inset of Figure 5, there is an increase in the Ds of Au atoms in the uncoated NP, albeit in a small scale, before the melting point. This increase in the D observed before the melting is an indication that a surface melting has occurred in the NP. However, the D of the coated NPs is around zero before the melting point as in the bulk system, indicating that they melt homogeneously without performing surface melting. These results show that the epitaxial Au/Pd interfaces formed in NP-1 and NP-2 with the core (Au)/shell (Pd) structure suppress the surface melting and delay the liquid nucleation, causing the NP to overheat. This effect becomes even more effective as the thickness of the shell (ie, as the number of Pd atoms increases). Because the melting point of NP-2, which has a larger shell thickness, is 1140 K, while the melting point of NP-1 is 1050 K.

The simplest way to examine the dynamic behavior of NPs during the heating process is to analyze snapshots of the atomic order at different temperatures. Snapshots of the atomic configuration taken at different temperatures for each NP are shown in Figure 6.
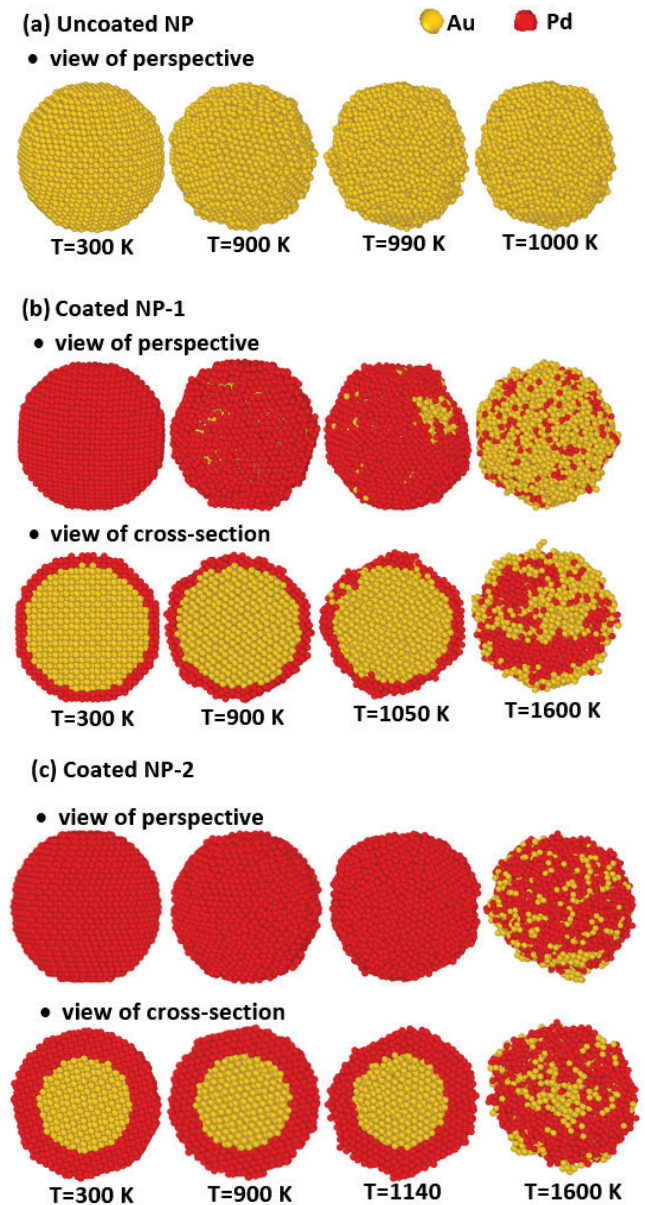

Fig. 6. *Snapshots of atomic configurations of (a) uncoated NP, (b) coated NP-1 (c) coated NP-2 at different temperatures.*

As can be seen from the images, all NPs retain their crystalline form at 300 K. With increasing temperature, the distance between atoms increases and metallic-bonds are broken. This causes the atomic order to be disrupted. In addition, the cross-section views show that the core/shell structure of NP-1 and NP-2 is disrupted at temperatures above the melting point due to the increased diffusive motion.

548

CONCLUSION

In this study, the structural and dynamic properties of Au NPs with Pd-coating were investigated during the melting process using classical MD simulation with QSC potentials. The results show that the uncoated Au NP melts at a lower temperature than the coated Au NPs. This can be explained by the fact that the epitaxial Au/Pd interfaces formed in the NP with the core/shell structure suppress the surface melting, leading to overheating of the coated NP. In addition, this effect becomes more effective depending on the thickness of the shell (ie, as the number of Pd atoms increases) and plays an important role on the thermal stability of the NP. While the coated NPs maintain their initial core/shell structures up to their melting temperatures, the volume of the NP increases with the increase of the interatomic distance after the melting. This causes the crystal structure to deteriorate and the core/shell diffusion to take place more intensely.

REFERENCE

[1] S. Alayoglu, F. Tao, V. Altoe, Catal. Lett., 141 (5), 633-640 (2011).

[2] Chaudhuri R. Gh., Chem. Rev., 112 (4), 2373–2433 (2012).

[3] W. Y. Yu, G. M. Mullen, D. W. Flaherty, J. Am. Chem. Soc., 136 (31), 110070-11078 (2014).

[4] H. Gleiter, Acta Mater., 48, 1 (2000).

[5] M. Alcoutlabi and G.. B. McKenna, J. Phys.: Condens. Matter., 17, 461 (2005).

[6] H. Jiang, K. Moon, H. Dong, F. Hua, and C. P. Wong, Chem. Phys. Lett., 429, 492 (2006).

[7] S. J. M. Rosales, C. F. Navarro, E. P. Tijerina, Phys. Chem. B., 110 (26), 12884–12889 (2006).

[8] M. Tsuji, N. Miyamae, S. Lim, Cryst. Growth Des., 6 (8), 1801–1807 (2006).

[9] S. W. Baek, G. Park, J. Noh Nano., 8 (4), 3302–3312 (2014).

[10] I. A. Lyashenko, V. N. Borysiuk, N. N. Manko, Cond. Matt. Phys., 17, 23003: 1– 11 (2014).

[11] Z. Yang, X. Yang, Z. Xu, J. Phys. Chem. C., 112 (13), 4937–4947 (2008).

[12] J. Broughton, Phys. Rev. Lett., 67, 2990 (1991).

[13] Z. H. Jin, H. W. Sheng, and K. Lu, Phys. Rev. B, 60, 141 (1999).

[14] L. Zhang, Z. H. Jin, L. H. Zhang, M. L. Sui, and K. Lu, Phys. Rev. Lett., 85, 1484 (2000).

[15] J. Broughton, Phys. Rev. B, 46, 2523 (1992).

[16] U. Shvets, V. Borysiuk, B. Natalich, Int. Sc. J. Math. Model., III (2), 66-69 (2019).

[17] D. W. Shi., L. M. He, L. G. Kong, H. Lin and L. Hong, Chin. J. Phys., 47 (4) 502-510 (2009).

[18] W. Smith, T.R. Forester, J. Mol. Graph. 14, 136–141 (1996).

[19] A.P. Sutton, J. Chen, Philos. Mag. Lett. 61, 139–146 (1990).

[20] T. Çagın, Y. Qi, H. Li, Y. Kimura, H. Ikeda, W. L. Jonhson, and W. A. Goddard III, MRS Symp. Ser. 554, 43 (1999).

[21] U. Domekeli, S. Sengul, M. Celtek, C. Canan., Philos. Mag. 98, 371–387 (2018).

[22] S. Nose, J. Chem. Phys. 81, 511–519 (1984).

[23] H. J. C. Berendsen, J. P. M. Postma, W.F. van Gunsteren, A. Di Nola, J. R. Haak, J. Chem. Phys. 81, 3684–3690 (1984).

[24] Y. Waseda, The Structure of Non-Crystalline Materials-Liquids and Amorphous Solids. New York: London: McGraw-Hill, (1981).

[25] C. Kittel, Introduction to Solid State Physics. New York: John Wiley & Sons Inc., (1986).